JACS
JOURNAL OF THE AMERICAN CHEMICAL SOCIETY
Article
pubs.acs.org/JACS

Precise Control of Quantum Dot Location within the P3HT-*b*-P2VP/QD Nanowires Formed by Crystallization-Driven 1D Growth of Hybrid Dimeric Seeds

Yong-Jae Kim,[†,∥] Chul-Hee Cho,[‡,∥] Kwanyeol Paek,[‡] Mijung Jo,[†] Mi-kyoung Park,[†] Na-Eun Lee,[†] Youn-joong Kim,[†,§] Bumjoon J. Kim,*[,‡] and Eunji Lee*[,†,§]

[†]Graduate School of Analytical Science and Technology, Chungnam National University, Daejeon 305-764, Republic of Korea

[‡]Department of Chemical and Biomolecular Engineering, Korea Advanced Institute of Science and Technology (KAIST), Daejeon 305-701, Republic of Korea

[§]Division of Electron Microscopic Research, Korea Basic Science Institute, Daejeon 305-806, Republic of Korea

Supporting Information

ABSTRACT: Herein, we report a simple fabrication of hybrid nanowires (NWs) composed of a p-type conjugated polymer (CP) and n-type inorganic quantum dots (QDs) by exploiting the crystallization-driven solution assembly of poly(3-hexylthiophene)-*b*-poly(2-vinylpyridine) (P3HT-*b*-P2VP) rod−coil amphiphiles. The visualization of the crystallization-driven growth evolution of hybrid NWs through systematic transmission electron microscopy experiments showed that discrete dimeric CdSe QDs bridged by P3HT-*b*-P2VP polymers were generated during the initial state of crystallization. These, in turn, assemble into elongated fibrils, forming the coaxial P3HT-*b*-P2VP/QDs hybrid NWs. In particular, the location of the QD arrays within the single strand of P3HT-*b*-P2VP can be controlled precisely by manipulating the regioregularity (RR) values of P3HT block and the relative lengths of P2VP block. The degree of coaxiality of the QD arrays was shown to depend on the coplanarity of the thiophene rings of P3HT block, which can be controlled by the RR value of P3HT block. In addition, the location of QDs could be regulated at the specific-local site of P3HT-*b*-P2VP NW according to the surface characteristics of QDs. As an example, the comparison of two different QDs coated with hydrophobic alkyl-terminated and hydroxyl-terminated molecules, respectively, is used to elucidate the effect of the surface properties of QDs on their nanolocation in the NW.

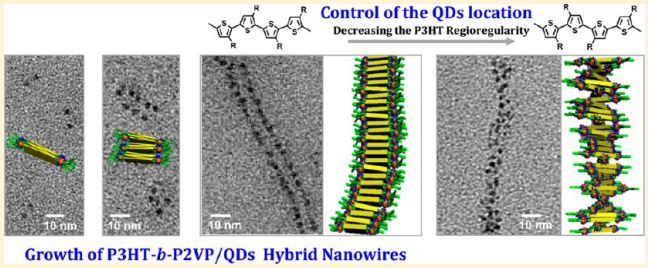

INTRODUCTION

Nanostructured hybrid materials composed of π-conjugated polymers (CPs) and inorganic nanoparticles (NPs) have attracted growing interest for developing next-generation electro-optical devices to deliver efficient energy conversion with low fabrication costs.[1−5] A variety of synthetic CPs have been utilized for the fabrication of thin-film devices with enhanced solution processability and flexibility.[6−9] Careful selection of inorganic NPs with well-matched energy levels for the CPs allows the hybrid system to show superior carrier mobility as well as photo- and chemical stability.[10] In particular, precisely controlled nanoscale morphology within the active layer enhances charge separation with a domain size comparable to the exciton diffusion length (~10 nm),[11,12] resulting in continuous charge transport pathway of electron-donating polymers and electron-accepting NPs with well-structured interface. In addition, the high crystallinity of materials is required to minimize losses during charge transport and thus improve the performance of organic/inorganic hybrid devices.[13] Indeed, thermal and solvent vapor annealings have typically been employed to improve the crystallinity of CPs in as-cast thin films of CPs and inorganic NPs.[14−17] However, inorganic NPs tend to aggregate intrinsically during processing, leading to macro-phase separation of the active layers, which minimizes the interfacial area between the polymer phase and the NPs.[18] It remains challenging to control the delicate balance between the nanoscale morphology and the molecular crystallinity of materials for producing high-performance hybrid devices.

To this end, the fabrication of one-dimensional (1D) organic−inorganic hybrid nanowires (NWs) driven by solution-state crystallization of CPs has been pursued.[19−21] Such fabrication could provide a well-segregated heterojunction between crystalline polymer and inorganic NPs within the nanoscale domain. For example, Gradečak and co-workers reported a thin-film-based solar cell consisting of CdS QDs-grafted poly(3-hexylthiophene) (P3HT) fibrils by solution-state noncovalent interactions, which produces a high power conversion efficiency (PCE) of 4.1% compared to a PCE of 0.6% for control sample of nongrafted CdS/P3HT-based films.[22] Recently, the Hayward and Emrick research groups

Received: October 3, 2013
Published: January 30, 2014

   dx.doi.org/10.1021/ja410165f | *J. Am. Chem. Soc.* 2014, 136, 2767−2774

Table 1. Characteristics of a Series of P3HT-*b*-P2VP Rod−Coil Diblock Copolymers

			P3HT		P3HT-*b*-P2VP	
polymer type	regioregularity[a]	P3HT:P2VP weight ratio[a]	M_n(g·mol^{-1})[b]	PDI[b]	M_n(g·mol^{-1})[b]	PDI[b]
rr-T1P1	92%	1:1	5800	1.18	10 500	1.57
ri-T1P1	78%	1:1	5200	1.42	10 000	1.69
rr-T1P3	92%	1:3	5800	1.18	23 200	1.81
ri-T1P3	78%	1:3	5200	1.42	19 800	1.65

[a]Determined from ^{1}H NMR. [b]From GPC in THF calibrated by polystyrene standards.

developed a new approach for fabricating p−n hybrid coaxial NWs in which P3HTs and P3HT-grafted CdSe nanorods were crystallized simultaneously in a mixed solvent.[20] Even more recently, microscale-long hybrid NWs were prepared through the modification of P3HT by end functionalization with thiol or phosphonic acid moieties.[21] The self-association of these CPs with the CdSe spheres or nanorods was shown to form multiple alternating arrays of the p-type fibrils and the n-type NPs. Based on these results, one can envision that understanding of the solution-state self-assembly process of CPs as well as further organization with inorganic NPs into extended arrays via bottom-up approaches would offer an efficient production means for organic−inorganic hybrid thin-film devices by coating and printing techniques without any annealing steps.

Meanwhile, extensive synthetic efforts have been devoted to the development of CPs to improve their crystallinity and solution processability. Incorporating flexible side chains with the conjugated backbone enables the fabrication of 1D NWs through solution-state assembly.[14,23,24] Integrating CPs with various polymer building blocks would provide the opportunity to control the mechanical, optoelectronic, and processing properties for device fabrication.[25−28] The degree of crystallinity of a NW could be determined by molecular parameters (e.g., molecular weight, polydispersity, and length of aliphatic side chains).[29] In particular, the regioregularity (RR) of polymer chains (i.e., the percentage of head-to-tail linkages between monomer units in the polymer backbone) has been identified as a key parameter governing thin-film morphology and subsequent charge delocalization.[30−33] However, under the conventional thermal treatment, several reports demonstrated that the utilization of polymers with high RR is not always the best way to fabricate a high-performance thin-film device.[34,35] For example, Fréchet and co-workers reported that the solar cell device of a higher RR-P3HT exhibited lower thermal stability.[35] During thermal annealing, induced crystallization of high RR-P3HT and of [6,6]-phenyl-C_{61}-butyric acid methyl ester (PCBM) within the active layer results in a larger extent of phase segregation between the two components, which leads to a decrease in device performance. Inspired by this, we asked whether the variation of P3HT-based block copolymer parameters including RR value of P3HT block and molecular weight would affect the fabrication of CP/QD hybrid NW with well-defined p−n junction by using the solution-state precrystallization method, enabling the improvement of the device performance and stability. The possibility of control of the QDs location has been investigated based on a fundamental understanding of the mutual assembly between polymer and inorganic NPs, providing the potential for manipulating optoelectronic properties of hybrid NW.

Herein, we demonstrate a simple and robust route to produce the hybrid NWs of poly(3-hexylthiophene)-*b*-poly(2-vinylpyridine) (P3HT-*b*-P2VP)/QDs with controlled nanolocation of QD array. The growth evolution of P3HT-*b*-P2VP with QDs into coaxial hybrid NWs was driven by solution-state self-assembly that was elucidated by systematic transmission electron microscopy (TEM) experiments. Significantly, the nanolocation of QD array into desired domains of the P3HT-*b*-P2VP NW can be precisely controlled by tuning (1) the RR value of the P3HT core block, (2) the relative lengths of the P2VP block, and (3) the surface chemistry of the QDs. To our best knowledge, this is the first report on the RR effect of P3HT polymer on the growth of nanocrystal fibrils of P3HT-based polymer, although the successful results with the solution-state fabrication of 1D hybrid nanostructures in previous studies.[20,21] Furthermore, for the first time, we demonstrate the control of QD locations within the coaxial hybrid NWs.

RESULTS AND DISCUSSION

Synthesis of P3HT-*b*-P2VP Polymers with Different P3HT RRs and P2VP Block Lengths. A series of P3HT-*b*-P2VP rod−coil polymers with different block lengths and P3HT RRs were synthesized as described in Schemes S1−3.[35−38] All molecular parameters of the P3HT-*b*-P2VP are summarized in Table 1. Polystyrene equivalent number-average molecular weights (M_n) and polydispersities (PDIs) were estimated by gel permeation chromatography (GPC) in THF. RR values of P3HT blocks were determined from ^{1}H NMR spectroscopy by comparing the integrated peaks that correspond to the α-methylene protons on the hexyl chains in head-to-tail (H−T) versus head-to-head (H−H) linkages, δ 2.81 and δ 2.58, respectively (Figures S1−5).[39] The four diblock copolymers were studied in detail. They had similar M_n numbers but different RR values of 92 and 78% in P3HT block. And, two different molecular weights of P2VP blocks were used, producing different P3HT:P2VP weight ratios (1:1 and 1:3) (denoted as rr-T1P1, ri-T1P1, rr-T1P3, and ri-T1P3, respectively, Table 1).

Self-Assembly Behavior of P3HT-*b*-P2VP into Nanofibrils in Mixed Solvents. The crystallization assembly of CPs can be induced by the addition of a poor solvent to a polymer solution in a good solvent.[40−42] Here, chloroform was used as a good solvent for both blocks of P3HT-*b*-P2VP, and acetonitrile was used as a selective solvent for the P2VP block. The formation of aggregates was confirmed by a color change of the solution from orange to purple (Figure 1a). The conformational change of the block copolymer from coil−coil to rod−coil can be attributed to avoiding unfavorable contacts between the P3HT block and acetonitrile, resulting in the self-assembly of polymers into aggregates.[43] Indeed, in chloroform, the single absorption peak of rr-T1P1 at a maximum at 438 nm showed the existence of isolated polymer chains (Figure S6a). When increasing the content of acetonitrile in solution, the absorption at 438 nm declined progressively, while vibronic bands at 508, 550, and 605 nm appeared, indicating the

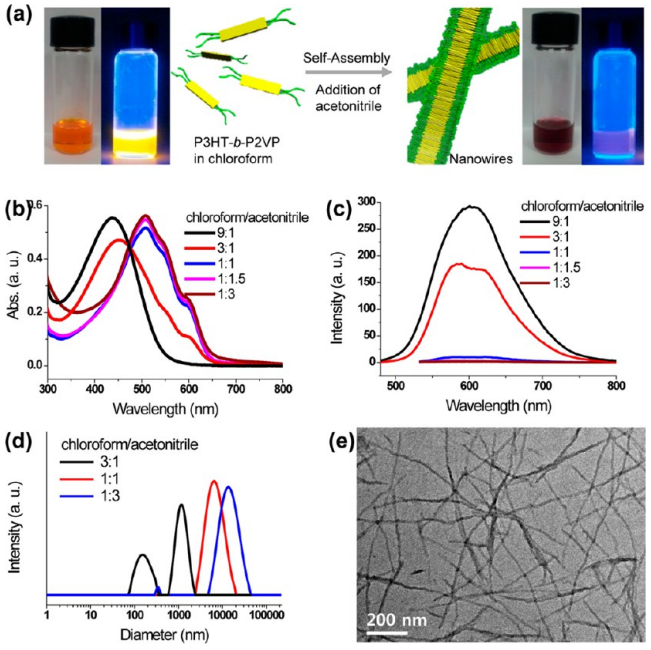

Figure 1. (a) Schematic representation of crystallization-driven NW formation of P3HT-*b*-P2VP rod−coil amphiphilic polymer. (b) Absorbance and (c) PL spectra of rr-T1P1 polymers dissolved in the mixed solvent as a function of solvent ratios (0.1 mg/mL). (d) Hydrodynamic radius of rr-T1P1 from DLS at different chloroform/acetonitrile ratios. (e) TEM image of rr-T1P1 NWs with micrometer-scale lengths (in chloroform/acetonitrile = 1:1, v/v).

formation of a crystal structure in which the planar thiophene backbones are stacked by face-to-face π-interactions (Figure 1b).[43−45] The distinct isosbestic point at 474 nm indicates the presence of isolated rr-T1P1 chains and aggregates. The progressive quenching of fluorescence intensity as the content of acetonitrile increased in the chloroform/acetonitrile mixture further showed the presence of strong $\pi-\pi$ interchain interactions in the assemblies (Figure 1c).

To corroborate the crystallization assembly of rr-T1P1 in the chloroform/acetonitrile mixture, dynamic light scattering (DLS) was performed with analysis using the CONTIN method (Figure 1d). The autocorrelation function of rr-T1P1 in a 9:1 chloroform/acetonitrile mixture (1 mg/mL) did not show any apparent aggregations. In a 3:1 mixed solution of chloroform and acetonitrile, a bimodal size distribution developed, with average sizes of 150 and 1162 nm. When the content of acetonitrile was further increased, the average hydrodynamic radii (R_H) increased more than ∼1 μm, reflecting the growth of the crystallized aggregates. When a sample was cast from the mixed solution (0.5 mg/mL), the TEM image of rr-T1P1 clearly shows the formation of the dark, micrometer-long 1D wires with a width of ∼9 nm (Figure 1e).[46]

Influence of P3HT RRs and Relative Block Lengths on the Formation of P3HT-*b*-P2VP NWs. The crystalline behavior of P3HT-*b*-P2VP fibrils, depending on the variation of P3HT RR, was investigated using UV−vis and fluorescence spectroscopies. The vibronic absorption of ri-T1P1 with a lower RR of 78% was significantly suppressed with respect to rr-T1P1 (Figure 2a). Although the photoluminescence (PL) intensity of ri-T1P1 in chloroform/acetonitrile was quenched when compared to those in chloroform (Figure S6b), it was much stronger than that of rr-T1P1 (Figure 2a). In the P3HT-*b*-

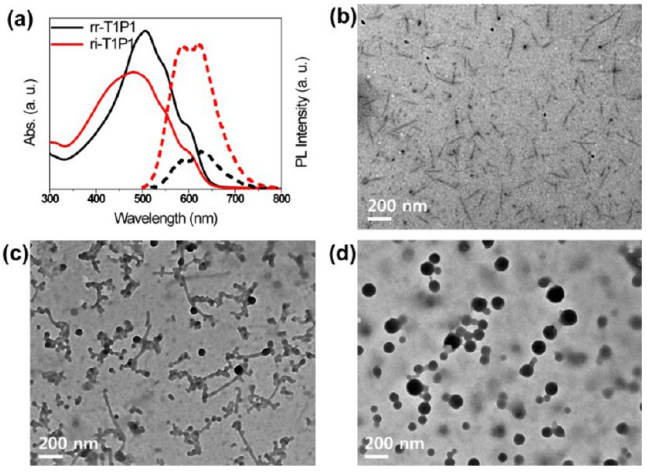

Figure 2. (a) Absorbance (solid line) and PL (dotted line) spectroscopies of rr-T1P1 and ri-T1P1 dissolved in the 1:1 chloroform/acetonitrile (0.1 mg/mL). TEM images of (b) ri-T1P1, (c) rr-T1P3, and (d) ri-T1P3 (0.5 mg/mL of chloroform/acetonitrile mixture).

P2VP solution self-assembly, efficient PL quenching is indicative of the presence of tightly packed P3HT and strong interchain couplings.[47] Thus, the larger distortion of the thiophene rings out of coplanarity imposed on the regioirregular P3HT may frustrate the growth of NWs.[32] To visualize directly the structural changes in terms of the P3HT RR, TEM experiments were performed with a 1:1 chloroform/acetonitrile solution of ri-T1P1. As expected, ri-T1P1 clearly formed much shorter fibrils with a length of several hundred nanometers (Figure 2b). Therefore, we concluded that the H−H couplings in regioirregular P3HT-*b*-P2VP induced a strong steric hindrance between thiophene rings, resulting in the reduction of effective intermolecular π-stacking of P3HT chains and the lack of 1D crystalline assembly.

Next, the effect of the P2VP length on the solution-assembly of P3HT-*b*-P2VP was investigated. The assembled morphology of π-conjugated rod−coil block copolymers should be strongly associated with the balance between the Flory−Huggins interaction (χN) and the Maier−Saupé type rod−rod interaction (μN), and the chain entropy.[48,49] Along this line, to keep the density of the P3HT-*b*-P2VP crystalline NW, the P2VP chains would face increasing steric repulsion with increasing the molecular weight, resulting in the dissociation of long fibrous crystals into smaller aggregates. To address this, rr- and ri-T1P3 polymers with a weight ratio of 1:3 P3HT:P2VP were synthesized. The length of the P2VP block was increased while keeping the length of P3HT constant (Table 1). Remarkably, the deformation of elongated fibrils was gradually observed, and the spherical aggregates appeared as the P2VP block length increased (Figure 2c). This result can be understood by considering the relative length of solvophobic P3HT and solvophilic P2VP. The increment of solvent-swollen P2VP corona favors a maximum degree of curvature at the core−corona interface, hampering the π-interactions between the neighboring P3HT core blocks. This results in the formation of spherical aggregates. At the same time, the decrease in the P3HT crystallinity of the assembled structure was reflected in the reduction of vibronic absorption (Figure S8a).[50] A complete structural transformation from fibrils into spheres was driven by a decrease in the RR of the P3HT block. The ri-T1P3 has been shown to self-assemble into spheres

dx.doi.org/10.1021/ja410165f | J. Am. Chem. Soc. 2014, 136, 2767−2774

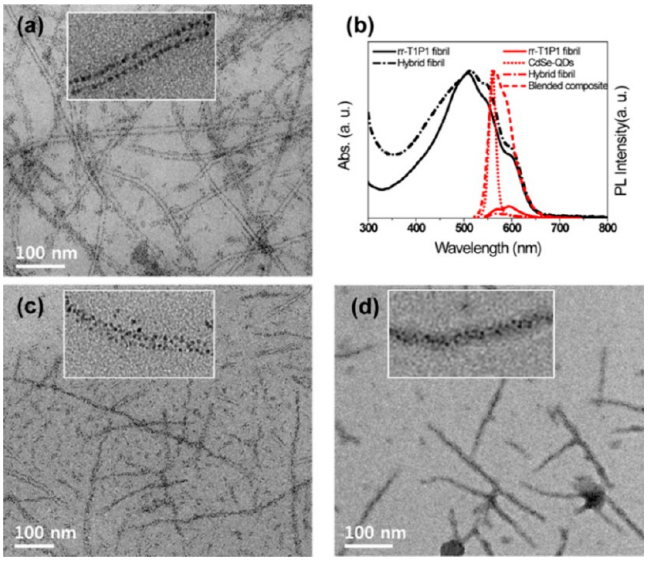

Figure 3. Hybrid NWs by cocrystallization of P3HT-*b*-P2VP and CdSe QDs: (a) TEM image of rr-T1P1/TOPO-capped CdSe QDs NWs. (b) Absorption and PL spectra of rr-T1P1 NW and rr-T1P1/QDs composite and wires. (c,d) TEM images showing nanohybrids of ri-T1P1/QDs and rr-T1P3/QDs, respectively.

ranging from 70 to 150 nm in size (Figure 2d). The decrease in the planarity and π-interaction of the 78% RR P3HT core block results in the additional loss of the 1D crystalline nature, which is well reflected in the enhancement of the emission intensity of ri-T1P3 compared with that of rr-T1P3 (Figure S8). These results indicated that the optical properties of π-conjugated rod−coil amphiphilic block copolymers related to their self-assembled structures are highly dependent on the conformational changes and the extent of π-interactions between neighboring conjugated chains.

Effect of P3HT RR and Relative Block Lengths on the Fabrication of P3HT-*b*-P2VP/CdSe-TOPO QDs Coaxial Hybrid NWs. The strong tendency of P3HT-*b*-P2VP to form crystalline NWs in chloroform/acetonitrile stimulated us to investigate whether organic−inorganic p−n hybrid NWs could be generated simply by coassembly of P3HT-*b*-P2VP and surface-modified n-type QDs. To fabricate the hybrid 1D NWs, the local sites of the core−shell P3HT-P2VP fibrous aggregates can be utilized through the interaction with surface modified inorganic QDs. First, tri-*n*-octyl phosphine oxide (TOPO) capped CdSe QDs with a diameter of about 3 nm were prepared (Figure S9).[51] The solvophobic interaction between the aliphatic chains on the QDs and the hexyl side chain of the P3HT block by addition of pure acetonitrile into the chloroform solution could lead to the co-organization of both components. The micronmeter-long P3HT-*b*-P2VP/QDs hybrid wires are successfully formed (Figure 3a). Interestingly, the QDs were associated into a single strand of rr-T1P1/QDs hybrid NW, producing well-ordered QDs parallel to the long axis of the fibrils.[20] The interparticle distance of rr-T1P1/QDs hybrid NW is of ∼9 nm, which is similar to a width of rr-P3HT homopolymer (M_n, 5800 g/mol) NW. Control experiments were conducted to investigate the factors governing such location of QDs within the hybrid NWs. Addition of CdSe-TOPO QDs into the preformed NWs of either rr-P3HT homopolymer or rr-T1P1 in the mixed chloroform/acetonitrile (1/1, v/v) solvent showed no association of QDs with NWs (Figures S10a−c and S11a). The coassembly of rr-P3HT and QDs in the mixed solvent formed the hybrid NWs where the QDs were randomly attached on the surface of NWs (Figures S10d,e). These results suggested that coassembly process is important for forming the hybrid NW, and the P2VP block might be expected to drive the QDs into both sides of NW. The presence of the vibronic absorption spectrum of the mixture at 605 nm confirms the formation of the crystalline fibrils even when QDs are incorporated (Figure 3b). The strong PL quenching of the hybrid chloroform/acetonitrile solution suggests an induction of charge and energy transfers between P3HT block and QDs, which is a stark contrast to those of P3HT-*b*-P2VP in chloroform/acetonitrile and a simply blended composite of P3HT-*b*-P2VP/QDs in chloroform. This result indicates the intimate contact between the donor and acceptor species by the formation of P3HT-*b*-P2VP/QDs coaxial NWs (Figure 3b).

A deeper insight into the self-assembly behavior of the P3HT-*b*-P2VP/QDs hybrid NWs can be obtained by investigating the effect of the RRs of the P3HT block and the relative block lengths of P3HT-*b*-P2VP on the NW morphology. The ri-T1P1 and rr-T1P3 polymers were employed to make a hybrid system with QDs. Interestingly, the TEM image of ri-T1P1/CdSe QDs hybrids showed the formation of QD-blended fibrils with a width of 9 nm (Figure 3c). The CdSe QDs appeared along the fibrils but are not arranged in a continuous linear path, which showed a contrast to the lined QD array in rr-T1P1 fibril. It could be speculated that the decrease in P3HT RR value of ri-T1P1 results in the reduced coplanarity of the thiophene rings with decreased interchain $\pi-\pi$ interactions between the ri-T1P1 chains. This feature combined with the steric constraint of the bulky QDs attached to the end of P3HT block could allow the mutual rotation of neighboring polymer chains in the same direction to form the fibrils with less ordered QD array. In addition, the hybridization of rr-T1P3 with a longer P2VP block length and QDs revealed to form a mixture of spherical aggregates and short fibrils with a width of ∼14 nm and a length of up to several hundred nanometers (Figure 3d). Interestingly, the CdSe QDs were localized preferentially within a central area of the NW with a width of 6−7 nm. The significant loss of the coaxiality of QDs in the NW can be explained by the increased steric demands of the longer P2VP block at the rr-T1P3 fibril edges. Therefore, it can be concluded that CdSe-TOPO QDs have a strong tendency to interact with the P3HT block, and the arrangement of QDs is strongly dominated by the crystallization assembly of P3HT-*b*-P2VP.

Different from the previously reported P3HT/CdSe QDs hybrid NWs by Xu et al.,[19] one of the main driving forces for the formation of coaxial hybrid NWs of P3HT-*b*-P2VP/CdSe QDs could be assumed to be the attractive interactions between aliphatic chains of QDs and hexyl side chain of P3HT rather than the coordination interaction between the sulfur atom of P3HT and the surface of the CdSe QDs. To this end, we investigated the mechanism for the formation of the hybrid NWs by examining their morphology at different growth stages. Specifically, at the early stage of the self-assembly process for hybridization, the isolated dimers of CdSe NPs with a center-to-center distance of about 8 nm were very often observed (Figure 4a). Interestingly, at the later stage of the growth, the dimers were stacked on each other in a 1D way, but the interparticle distance was still preserved (Figures 4b,c). The average diameter of NWs was increased up to 7410 nm after 24h, and there was no significant difference between 24 and 36

dx.doi.org/10.1021/ja410165f | J. Am. Chem. Soc. 2014, 136, 2767−2774

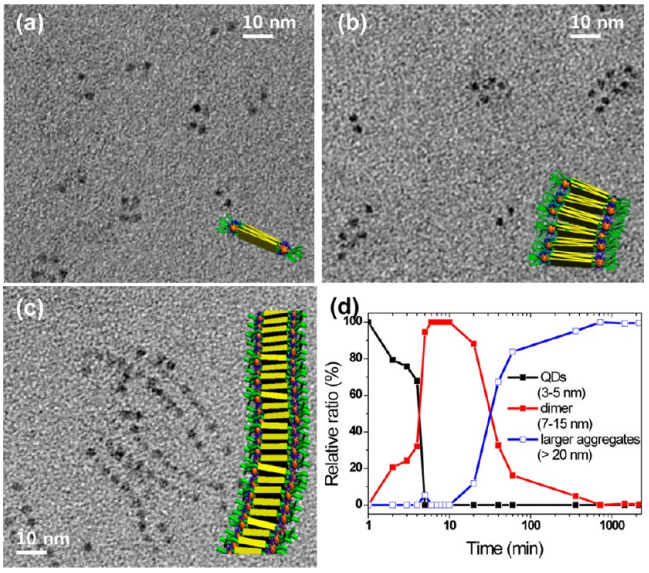

Figure 4. (a–c) Structural evolution of the formation of hybrid NW from the self-assembly of QD dimeric seeds bridged by rr-T1P1. (d) Time course of the relative ratio changes of rr-T1P1/QD dimers to larger aggregates in hydrodynamic diameter monitored using DLS (0.5 mg/mL in chloroform/acetonitrile).

h (Figures 4d and S13). As the interparticle distance of the dimers corresponds to that of the resulting rr-T1P1/CdSe-TOPO hybrid NWs, it could be concluded that the QD dimers are first bridged by P3HT-*b*-P2VP polymers by solvophobic interactions and then evolved to form fibrils consisting of stacks of the QD dimers in order to avoid unfavorable contact between the P3HT block and acetonitrile molecules. If the coordination interactions were a major driving force in the hybridization of P3HT-*b*-P2VP with QDs, the randomly attached multiple QDs-polymer crystal seeds would have been observed instead. In detail, it can be proposed that P3HT-*b*-P2VP polymers are assembled to form the elemental polymer crystal seeds with a dimer of QDs in the initial state. In turn, these seeds are organized into 1D NWs through face-to-face π-stacking of the crystal seeds. The hybrid NWs need at least a day to grow into a stable colloidal structure (Figure 4d) and remain well-dispersed over long periods of time, generally several weeks, under dark conditions. Such a slow assembly to reach an equilibrium state of polymer crystallization could provide a model system for visualizing and characterizing the crystallization assembly process of CPs.

Control of the Site Localization of the QDs within the Hybrid Nanowires by Surface Modification. Averaged over 150 rr-T1P1/CdSe-TOPO hybrid NWs, the center-to-center interparticle distance of 9.1 ± 0.5 nm was determined from the TEM images (Figure 5a). The TEM image with selective I_2 staining for the P2VP domain showed that the QDs were strongly localized at the borderline between the P3HT and P2VP domains (Figure 5b).[52] The control of the QD location within the CP/QD hybrid nanostructures is critically important to determine their optical, electrical, and electronic properties because their energy and charge transfers from polymer to QDs are strongly dependent on the interdistance between two different species.[53,54] However, to our best knowledge, the control over the nanolocation of the NPs within the hybrid polymer NWs has not been reported. In this regard, we modified the surface properties of the QDs. This approach

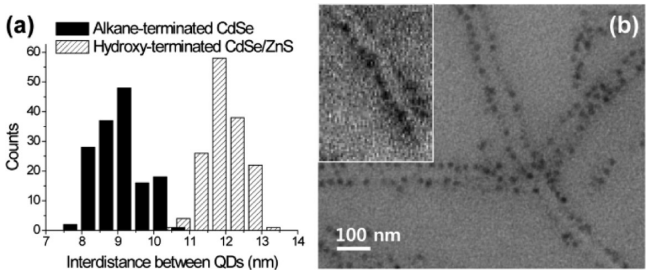

Figure 5. (a) Distributions of interparticle distance between alkane-terminated QDs (CdSe-TOPO QDs) and hydroxyl-terminated QDs (MCH/DDT-covered QDs) within the rr-T1P1/QDs hybrid NWs, respectively. (b) Selective staining of the P2VP domain of P3HT-*b*-P2VP fibrils with I_2.

utilizes the specific, strong nonconvalent interactions between one of the polymer blocks and the QD surface,[55] producing the selective incorporation of QDs into the desired domains with controlled nanolocation within the 1D NWs.[56,57] To demonstrate this, 6-mercapto-1-hexanol (MCH)-functionalized CdSe/ZnS QDs with a diameter of 4 nm were prepared, which can interact favorably with the pyridine moiety of the P2VP block through the formation of hydrogen bonding (Figure S14).[58] Since CdSe/ZnS QDs covered solely by MCH molecules were not dissolved in chloroform and acetonitrile, a mixture of MCH and dodecanthiol (DDT) with a ratio of 8:2 was used to produce hydroxyl-terminated QDs. The composition of the ligands on the QDs was controlled by the concentration of MCH used in the ligand exchange.[59]

As shown in Figure 6a, P3HT-*b*-P2VP/hydroxyl terminated QDs hybrid coaxial NWs were successfully generated by solvent removal from chloroform/acetonitrile solution-cast films. The center-to-center distance between the CdSe/ZnS QDs arrays within a single NW was determined to be 12.0 ± 1.4 nm, indicating the successful localization of CdSe/ZnS QDs in the P2VP domain (Figure 5a). It should be noted that the interparticle distance of the hydroxy-terminated QDs in the rr-T1P1/QDs hybrid NWs had ~3 nm increase compared to that of the rr-T1P1/CdSe-TOPO QDs hybrid NWs. Considering the conformation of the P3HT-*b*-P2VP chains in the NW and the length of P2VP blocks, the increase of 3 nm in the center-to-center distance should reflect the change in the CdSe/ZnS QDs location from the P3HT/P2VP interface into the P2VP domain. Further evidence of the specific localization of the QDs in P2VP domain can be provided by FT-IR measurements that monitor the presence of hydrogen bonding in the thin films generated by drop casting of the rr-T1P1/QDs solution.[60−62] In the spectra of 3000−3600 cm^{-1} region, the absorption band peak at 3319 cm^{-1} indicated the presence of hydroxy groups originated from the MCH ligands on the CdSe/ZnS NPs (Figure 6b). Upon hybridization with rr-T1P1, the original peak shifted to a lower wavenumber, and a new absorption peak appeared at 3291 cm^{-1} via hydrogen bonding between pyridine groups on the rr-T1P1 and the hydroxy groups on the CdSe/ZnS QDs. In addition, the absorbance decreased at 993 cm^{-1}, which corresponds to the free pyridine; instead, the absorbance increased at 1001 cm^{-1} due to the formation of the hydrogen-bonded pyridine by the increased addition of MCH ligands on the QDs (Figure 6c).[61] The shift in the position of the original peak to a higher wavenumber can be explained by the fact that the pyridine rings became more rigid upon hydrogen bonding.[63] The degree of shift was shown to depend

dx.doi.org/10.1021/ja410165f | J. Am. Chem. Soc. 2014, 136, 2767−2774

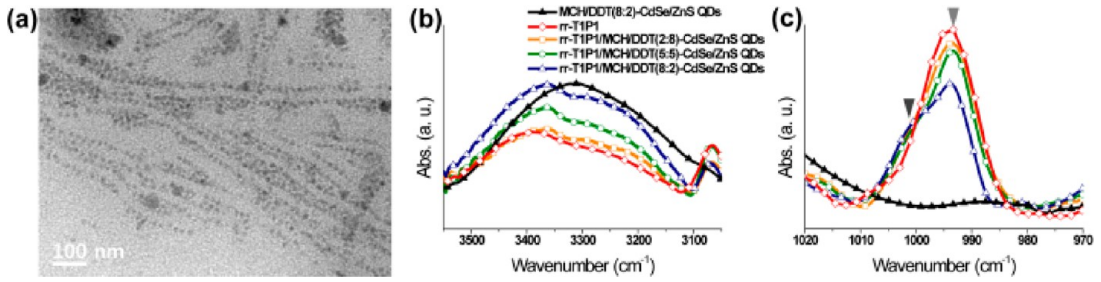

Figure 6. (a) TEM image of hybrid NWs of rr-T1P1 with hydroxyl-terminated CdSe/ZnS QDs. FT-IR spectra of the rr-T1P1, MCH/DDT (8:2) capped-CdSe/ZnS QDs, and rr-T1P1/CdSe/ZnS QDs with different ratios of MCH to DDT: regions between (b) 3000 and 3600 cm^{-1} and (c) 970 and 1020 cm^{-1}.

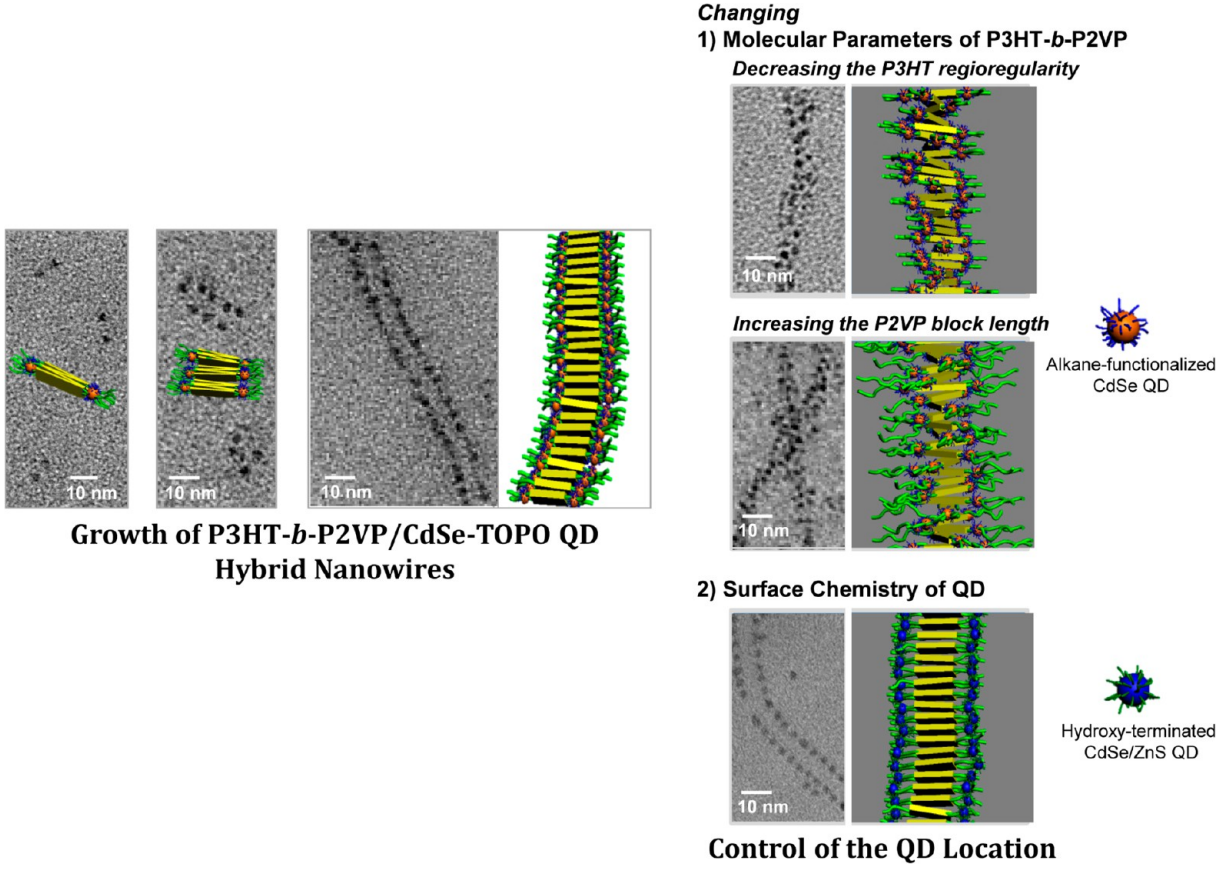

Figure 7. Growth of P3HT-*b*-P2VP/QD dimeric seeds into 1D hybrid NWs in mixed solvent of chloroform and acetonitrile, and control of the QD location within the NW by changing the molecular parameters of P3HT-*b*-P2VP and surface chemistry of QD.

on the ratios of MCH to DDT, demonstrating that the QDs can be well-incorporated into specific local sites of core−shell NWs by surface modification. Indeed, the coaxial hybrid NWs have also been fabricated by adding MCH/DDT-capped QDs to a suspension of precrystallized rr-T1P1 NWs in contrast to adding CdSe-TOPO QDs (Figures S11). It seems to be attributed to the exposed P2VP block at the peripheral site of precrystallized rr-T1P1 NWs that facilitate hydrogen-bonding formation between the pyridine group of P2VP and MCH ligand of QD.

Finally, analytical TEM measurements were performed to confirm the site-selective localization of QDs within the hybrid NWs (Figure S15). The high-angle annular dark-field scanning TEM (HAADF-STEM) indicated a clear contrast between the QDs and the P3HT-*b*-P2VP block copolymer due to the large differences in atomic numbers. The position marked in the box in Figure S15a of the energy dispersive X-ray spectroscopy (EDX) indicates the existence of cadmium and selenide, while the box in Figure S15c shows the presence of not only cadmium and selenide but also zinc and sulfur. As a result, these observations support the notion that hydroxy- or alkane-terminated QDs are well-incorporated into P3HT- *b*-P2VP NWs via hydrogen bonding or solvophobic interaction, respectively.[59] The coaxial hybrid NWs reported previously should require the surface functionalization of QDs with P3HT-based polymer grafting for use with the cocrystallization method.[20] In this work, simple hydrophilic or hydrophobic surface modifications of NPs enabled the fabrication of hybrid NWs by using the crystallization-driven solution self-assembly. Therefore, controlling the surface chemistry of NPs can be one of the most important factors in generalizing the precrystallization method for the fabrication of a 1D hybrid nanostructure.

dx.doi.org/10.1021/ja410165f | J. Am. Chem. Soc. 2014, 136, 2767−2774

CONCLUSION

NWs of P3HT-*b*-P2VP rod−coil amphiphilic block copolymers were fabricated by solution-state crystallization assembly, which was capable of generating well-ordered QD hybrid structures through noncovalent interactions. The self-assembly behavior for hybrid NWs was driven by the crystallization of the P3HT block core in the mixed solvent consisting of chloroform and acetonitrile. The lengths of both the bare and hybrid fibrils could be controlled by tuning the RR numbers of the P3HT block and the relative block lengths, which affected the extent of crystallization of the P3HT block. Interestingly, hybrid NWs based on the P3HT-*b*-P2VP with highly regioregular P3HT revealed a coaxial arrangement of QDs along the fibril axis with their controlled location. More interestingly, at the initial state of the P3HT-*b*-P2VP hybridization assembly with QDs toward 1D NWs, the finding that the QD dimers were bridged by polymers provides an opportunity to infer a growth mechanism for coaxial P3HT-*b*-P2VP/QDs hybrid NWs. The coaxiality of QDs within the hybrid NW was controlled by varying the polymer parameters including RR values and relative block lengths. In addition, the localization of QDs within the desired domains of hybrid NWs can be controlled precisely by the surface modification of QDs. These results suggest that the precrystallization of a regioregular P3HT-based polymer for the fabrication of 1D hybrid NWs could provide effective highly crystalline, nanoscale domains without conventional solvent vapor or thermal annealing treatments. The fabrication methods and characterizations for both crystalline fibrils and their hybrid NWs offer a useful strategy for fine-tuning the optical and electrical properties of organic−inorganic hybrid materials as a solution-processed active layer in photovoltaic devices and thin-film transistors.

ASSOCIATED CONTENT

Supporting Information

Synthesis and identification of a series of block copolymers and QDs, and self-assembly behavior of rod−coil block copolymers and hybrids with QD. This material is available free of charge via the Internet at http://pubs.acs.org.

AUTHOR INFORMATION

Corresponding Authors

eunjilee@cnu.ac.kr
bumjoonkim@kaist.ac.kr

Author Contributions

‖These authors contributed equally.

Notes

The authors declare no competing financial interest.

ACKNOWLEDGMENTS

This research was supported by Basic Science Research Program (2013R1A1A2061197, 2013R1A2A2A04015914) through the National Research Foundation of Korea (NRF) funded by the Korean Government. This research was also supported by the Global Frontier R&D Program on Center for Multiscale Energy System (2012M3A6A7055540) funded by the Korean Government. Experiments at PLS (Beamline 9A) were supported in part by MSIP and POSTECH.

REFERENCES

(1) Greeham, N. C.; Peng, X.; Alivisatos, A. P. *Phys. Rev. B* **1996**, *54*, 17628−17637.
(2) Huynh, W. U.; Dittmer, J. J.; Alivisatos, A. P. *Science* **2002**, *295*, 2425−2427.
(3) Weickert, J.; Dunbar, R. B.; Hesse, H. C.; Wiedemann, W.; Schmidt-Mende, L. *Adv. Mater.* **2011**, *23*, 1810−1828.
(4) Zhou, R.; Stalder, R.; Xie, D.; Cao, W.; Zheng, Y.; Yang, Y.; Plaisant, M.; Holloway, P. H.; Schanze, K. S.; Reynolds, J. R.; Xue, J. *ACS Nano* **2013**, *7*, 4846−4854.
(5) Zhou, Y.; Eck, M.; Krüger, M. *Energy Environ Sci.* **2010**, *3*, 1851−1864.
(6) Arias, A. C.; MacKenzie, J. D.; McCulloch, I.; Rivnay, J.; Salleo, A. *Chem. Rev.* **2010**, *110*, 3−24.
(7) Krebs, F. C. *Sol. Energy Mater. Sol. Cells* **2009**, *93*, 394−412.
(8) Facchetti, A. *Chem. Mater.* **2011**, *23*, 733−758.
(9) Peet, J.; Heeger, A. J.; Bazan, G. C. *Acc. Chem. Res.* **2009**, *42*, 1700−1708.
(10) Kovalenko, M. V.; Scheele, M.; Talapin, D. V. *Science* **2009**, *324*, 1417−1420.
(11) Shaw, P. E.; Ruseckas, A.; Samuel, I. D. W. *Adv. Mater.* **2008**, *20*, 3516−3520.
(12) Thompson, B. C.; Fréchet, J. M. J. *Angew. Chem., Int. Ed.* **2008**, *47*, 58−77.
(13) Yang, X.; Loos, J. *Macromolecules* **2007**, *40*, 1353−1362.
(14) Xin, H.; Kim, F. S.; Jenekhe, S. A. *J. Am. Chem. Soc.* **2008**, *130*, 5424−5425.
(15) Padinger, F.; Rittberger, R. S.; Sariciftci, N. S. *Adv. Funct. Mater.* **2003**, *13*, 85−88.
(16) Li, G.; Shrotriya, V.; Huang, J.; Yao, Y.; Moriarty, T.; Emery, K.; Yang, Y. *Nat. Mater.* **2005**, *4*, 864−868.
(17) Ma, W.; Yang, C.; Gong, X.; Lee, K.; Heeger, A. J. *Adv. Funct. Mater.* **2005**, *15*, 1617−1622.
(18) Coe-Sullivan, S.; Steckel, J. S.; Woo, W.-K.; Bawendi, M. G.; Bulović, V. *Adv. Funct. Mater.* **2005**, *15*, 1117−1124.
(19) Xu, J.; Hu, J.; Liu, X.; Qiu, X.; Wei, Z. *Macromol. Rapid Commun.* **2009**, *30*, 1419−1423.
(20) Bokel, F. A.; Sudeep, P. K.; Pentzer, E.; Emrick, T.; Hayward, R. C. *Macromolecules* **2011**, *44*, 1768−1770.
(21) Pentzer, E. B.; Bokel, F. A.; Hayward, R. C.; Emrick, T. *Adv. Mater.* **2012**, *24*, 2254−2258.
(22) Ren, S.; Chang, L.-Y.; Lim, S.-K.; Zhao, J.; Smith, M.; Zhao, N.; Bulović, V.; Bawendi, M.; Gradečak, S. *Nano Lett.* **2011**, *11*, 3998−4002.
(23) Ihn, K. J.; Moulton, J.; Smith, P. *J. Polym. Sci., Part B: Polym. Phys.* **1993**, *31*, 735−742.
(24) Qiu, L. Z.; Lee, W. H.; Wang, X.; Kim, J. S.; Lim, J. A.; Kwak, D.; Lee, S.; Cho, K. *Adv. Mater.* **2009**, *21*, 1349−1353.
(25) Liu, J.; Sheina, E.; Kowalewski, T.; McCullough, R. D. *Angew. Chem., Int. Ed.* **2002**, *41*, 329−332.
(26) He, M.; Zho, L.; Wang, J.; Han, W.; Yang, Y.; Qiu, F.; Lin, Z. *ACS Nano* **2010**, *4*, 3241−3247.
(27) Lee, E.; Hammer, B.; Kim, J.-K.; Emrick, T.; Hayward, R. C. *J. Am. Chem. Soc.* **2011**, *133*, 10390−10393.
(28) Kim, H. J.; Paek, K.; Yang, H.; Cho, C.-H.; Kim, J.-S.; Lee, W.; Kim, B. J. *Macromolecules* **2013**, *46*, 8472−8478.
(29) Dang, M. T.; Hirsch, L.; Wantz, G.; Wuest, J. D. *Chem. Rev.* **2013**, *113*, 3734−3765.
(30) Kim, Y.; Cook, S.; Tuladhar, S. M.; Choulis, S. A.; Nelson, J.; Durrant, J. R.; Bradley, D. D. C.; Giles, M.; McCulloch, I.; Ha, C.-S.; Ree, M. *Nat. Mater.* **2006**, *5*, 197−203.
(31) Richter, T. V.; Braun, C. H.; Link, S.; Scheuble, M.; Crossland, E. J. W.; Stelzl, F.; Würfel, U.; Ludwigs, S. *Macromolecules* **2012**, *45*, 5782−5788.
(32) Osaka, I.; McCullough, R. D. *Acc. Chem. Res.* **2008**, *41*, 1202−1214.
(33) Tsao, H. N.; Müllen, K. *Chem. Soc. Rev.* **2010**, *39*, 2372−2386.
(34) Sivula, K.; Luscombe, C. K.; Thompson, B. C.; Fréchet, J. M. J. *J. Am. Chem. Soc.* **2006**, *128*, 13988−13989.
(35) Woo, C. H.; Thompson, B. C.; Kim, B. J.; Toney, M. F.; Fréchet, J. M. J. *J. Am. Chem. Soc.* **2008**, *130*, 16324−16329.

(36) Iovu, M. C.; Craley, C. R.; Jeffries-EL, M.; Krankowski, A. B.; Zhang, R.; Kowalewski, T.; McCullough, R. D. *Macromolecules* **2007**, *40*, 4733−4735.
(37) Kim, H. J.; Han, A.-R.; Cho, C.-H.; Kang, H.; Cho, H.-H.; Lee, M. Y.; Fréchet, J. M. J.; Oh, J. H.; Kim, B. J. *Chem. Mater.* **2012**, *24*, 215−221.
(38) Cho, C.-H.; Jung, D.-I.; Neuenswander, B.; Larock, R. C. *ACS Comb. Sci.* **2011**, *13*, 501−510.
(39) Lee, Y.-H.; Yen, W.-C.; Su, W.-F.; Dai, C.-A. *Soft Matter* **2011**, *7*, 10429−10442.
(40) Kiriy, N.; Jähne, E.; Adler, H.-J.; Schneider, M.; Kiriy, A.; Gorodyska, G.; Minko, S.; Jehnichen, D.; Simon, P.; Fokin, A. A.; Stamm, M. *Nano Lett.* **2003**, *3*, 707−712.
(41) Chen, J.-T.; Hsu, C.-S. *Polym. Chem.* **2011**, *2*, 2707−2722.
(42) Gwyther, J.; Gilroy, J. B.; Rupar, P. A.; Lunn, D. J.; Kynaston, E.; Patra, S. K.; Whittell, G. R.; Winnik, M. A.; Manners, I. *Chem.—Eur. J.* **2013**, *19*, 9186−9197.
(43) Samitsu, S.; Shimomura, T.; Heike, S.; Hashizume, T.; Ito, K. *Macromolecules* **2008**, *41*, 8000−8010.
(44) Park, Y. D.; Lee, H. S.; Choi, Y. J.; Kwak, D.; Cho, J. H.; Lee, S.; Cho, K. *Adv. Funct. Mater.* **2009**, *19*, 1200−1206.
(45) Brown, P. J.; Thomas, D. S.; Köhler, A.; Wilson, J. S.; Kim, J.-S.; Ramsdale, C. M.; Sirringhaus, H.; Friend, R. H. *Phys. Rev. B* **2003**, *67*, 064203.
(46) The preferential orientation of ordered P3HT chains of rr-T1P1 NW was confirmed by grazing incidence wide-angle X-ray scattering (GI-WAXS) measurement (Figure S7).
(47) Xu, B.; Holdcroft, S. *Macromolecules* **1993**, *26*, 4457−4460.
(48) Olsen, B. D.; Segalman, R. A. *Macromolecules* **2005**, *38*, 10127−10137.
(49) Sary, N.; Rubatat, L.; Brochon, C.; Hadziioannou, G.; Ruokolainen, J.; Mezzenga, R. *Macromolecules* **2007**, *40*, 6990−6997.
(50) Nagarjuna, G.; Baghgar, M.; Labastide, J. A.; Algaier, D. D.; Barnes, M. D.; Venkataraman, D. *ACS Nano* **2012**, *6*, 10750−10758.
(51) Peng, Z. A.; Peng, X. *J. Am. Chem. Soc.* **2001**, *123*, 183−184.
(52) Yen, W.-C.; Lee, Y.-H.; Lin, J.-F.; Dai, C.-A.; Jeng, U.-S.; Su, W.-F. *Langmuir* **2011**, *27*, 109−115.
(53) Lakowicz, J. R. *Principles of Fluorescence Spectroscopy*, 3rd ed.; Springer: New York, 2006.
(54) Paek, K.; Chung, S.; Cho, C.-H.; Kim, B. J. *Chem. Commun.* **2011**, *47*, 10272−10274.
(55) Jang, J.; Kim, J.-K.; Choi, J.-W.; Hwang, T.-S.; Jo, M.; Kim, I.; Cho, B.-K.; Lee, E. *Chem. Commun.* **2013**, *49*, 8003−8005.
(56) Chiu, J. J.; Kim, B. J.; Kramer, E. J.; Pine, D. J. *J. Am. Chem. Soc.* **2005**, *127*, 5036−5037.
(57) Kim, B. J.; Bang, J.; Hawker, C. J.; Chiu, J. J.; Pine, D. J.; Jang, S. G.; Yang, S.-M.; Kramer, E. J. *Langmuir* **2007**, *23*, 12693−12703.
(58) Bae, W. K.; Char, K.; Hur, H.; Lee, S. *Chem. Mater.* **2008**, *20*, 531−539.
(59) Li, Q.; He, J.; Glogowski, E.; Li, X.; Wang, J.; Emrick, T.; Russell, T. P. *Adv. Mater.* **2008**, *20*, 1462−1466.
(60) Jang, S. G.; Khan, A.; Hawker, C. J.; Kramer, E. J. *Macromolecules* **2012**, *45*, 1553−1561.
(61) Noro, A.; Higuchi, K.; Sageshima, Y.; Matsushita, Y. *Macromolecules* **2012**, *45*, 8013−8020.
(62) Jang, S. G.; Kramer, E. J.; Hawker, C. J. *J. Am. Chem. Soc.* **2011**, *133*, 16986−16996.
(63) Cesteros, L. C.; Isasi, J. R.; Katime, I. *Macromolecules* **1993**, *26*, 7256−7262.